

Gamma-Ray Bursts as a Probe of Cosmology

Donald Q. Lamb

Department of Astronomy & Astrophysics, University of Chicago, 5640 South Ellis Avenue, Chicago, IL 60637

Abstract. We show that, if the long GRBs are produced by the collapse of massive stars, GRBs and their afterglows may provide a powerful probe of cosmology and the early universe.

INTRODUCTION

There is increasingly strong evidence that gamma-ray bursts (GRBs) are associated with star-forming galaxies [1,2,3,4] and occur near or in the star-forming regions of these galaxies [2,3,4,5,6]. These associations provide indirect evidence that at least the long GRBs detected by BeppoSAX are a result of the collapse of massive stars. The discovery of what appear to be supernova components in the afterglows of GRBs 970228 [7,8] and 980326 [9] provides tantalizing direct evidence that at least some GRBs are related to the deaths of massive stars, as predicted by the widely-discussed collapsar model of GRBs [10,11,12,13,14]. If GRBs are indeed related to the collapse of massive stars, one expects the GRB rate to be approximately proportional to the star-formation rate (SFR).

DETECTABILITY OF GRBS AND THEIR AFTERGLOWS

We have calculated the limiting redshifts detectable by BATSE and HETE-2, and by *Swift*, for the sixteen GRBs with well-established redshifts and published peak photon number fluxes. In doing so, we have used the peak photon number fluxes given in Table 1 of [15], taken a detection threshold of 0.2 ph s^{-1} for BATSE and HETE-2 and 0.04 ph s^{-1} for *Swift*, and set $H_0 = 65 \text{ km s}^{-1} \text{ Mpc}^{-1}$, $\Omega_m = 0.3$, and $\Omega_\Lambda = 0.7$ (other cosmologies give similar results). Figure 1 displays the results. This figure shows that BATSE and HETE-2 would be able to detect half of these GRBs out to a redshift $z = 20$ and 20% of them out to a redshift $z = 50$. *Swift* would be able to detect half of them out to redshifts $z = 70$, and 20% of them out to a redshift $z = 200$, although it is unlikely that GRBs occur at such extreme redshifts. Consequently, if GRBs occur at very high ($z > 5$) redshifts (VHRs), BATSE has probably already detected GRBs

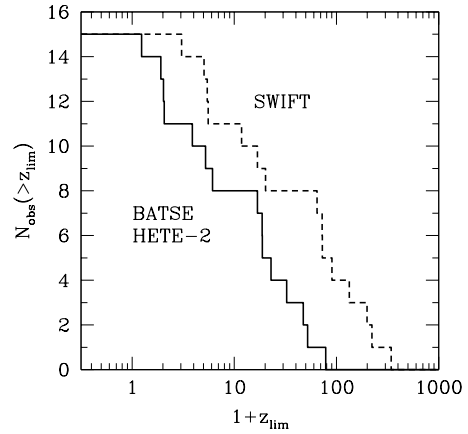


FIGURE 1. Cumulative distributions of the limiting redshifts at which the 15 GRBs with well-determined redshifts and published peak photon number fluxes would be detectable by BATSE and HETE-2, and by *Swift*.

at these redshifts, and HETE-2 and *Swift* should detect them as well.

The soft X-ray, optical and infrared afterglows of GRBs are also detectable out to VHRs. The effects of distance and redshift tend to reduce the spectral flux in GRB afterglows in a given frequency band, but time dilation tends to increase it at a fixed time of observation after the GRB, since afterglow intensities tend to decrease with time. These effects combine to produce little or no decrease in the spectral energy flux F_ν of GRB afterglows in a given frequency band and at a fixed time of observation after the GRB with increasing redshift:

$$F_\nu(\nu, t) = \frac{L_\nu(\nu, t)}{4\pi D^2(z)(1+z)^{1-a+b}}, \quad (1)$$

where $L_\nu \propto \nu^a t^b$ is the intrinsic spectral luminosity of the GRB afterglow, which we assume applies even at early times, and $D(z)$ is the comoving distance to the burst.

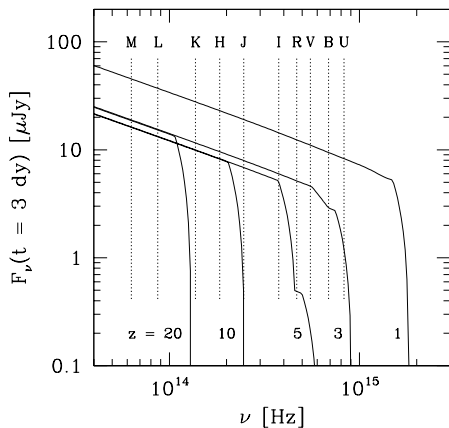


FIGURE 2. The best-fit spectral flux distribution of the early afterglow of GRB 000131, as observed one day after the burst, after transforming it to various redshifts, and extinguishing it with a model of the Ly α forest.

Many afterglows fade like $b \approx -4/3$, which implies that $F_v(\nu, t) \propto D(z)^{-2}(1+z)^{-5/9}$ in the simplest afterglow model, where $a = 2b/3$ [16]. In addition, $D(z)$ increases very slowly with redshift at redshifts greater than a few. Consequently, there is little or no decrease in the spectral flux of GRB afterglows with increasing redshift beyond $z \approx 3$.

In fact, in the simplest afterglow model where $a = 2b/3$, if the afterglow declines more rapidly than $b \approx 1.7$, the spectral flux actually *increases* as one moves the burst to higher redshifts! An example of this is the afterglow of GRB 000131. Its peak flux F_{peak} was in the top 5% of all BATSE bursts and the break energy E_{break} in its spectrum was 164 keV, yet it occurred at a redshift $z = 4.50$. We have calculated the best-fit spectral flux distribution of the afterglow of GRB 000131 from [17], as observed three days after the burst, transformed to various redshifts. The transformation involves (1) dimming the afterglow, (2) redshifting its spectrum, (3) time dilating its light curve, and (4) extinguishing the spectrum using a model of the Ly α forest (for details, see [15]). Finally, we have convolved the transformed spectra with a top hat smearing function of width $\Delta\nu = 0.2\nu$. This models these spectra as they would be sampled photometrically, as opposed to spectroscopically; i.e., this transforms the model spectra into model spectral flux distributions.

Figure 2 shows the resulting spectral flux distribution. The spectral flux distribution of the afterglow is cut off by the Ly α forest at progressively lower frequencies as one moves out in redshift. Thus high redshift afterglows are characterized by an optical “dropout” [4], and VHR afterglows by a near infrared “dropout.” We conclude that, if GRBs occur at very high redshifts, both they and

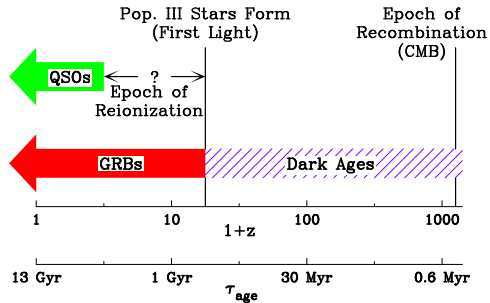


FIGURE 3. Cosmological context of VHR GRBs. Shown are the epochs of recombination, first light, and re-ionization. Also shown are the ranges of redshifts corresponding to the “dark ages,” and probed by QSOs and GRBs.

their afterglows can be easily detected.

GRBS AS A PROBE OF COSMOLOGY AND THE EARLY UNIVERSE

Theoretical calculations show that the birth rate of Pop III stars produces a peak in the SFR in the universe at redshifts $16 \lesssim z \lesssim 20$, while the birth rate of Pop II stars produces a much larger and broader peak at redshifts $2 \lesssim z \lesssim 10$ [18,19,20]. Therefore one expects GRBs to occur out to at least $z \approx 10$ and possibly $z \approx 15 - 20$, redshifts that are far larger than those expected for the most distant quasars.

Figure 3 places GRBs in a cosmological context. At recombination, which occurs at redshift $z = 1100$, the universe becomes transparent. The cosmic background radiation originates at this redshift. Shortly afterwards, the temperature of the cosmic background radiation falls below 3000 K and the universe enters the “dark ages” during which there is no visible light in the universe. “First light,” which occurs at $z \approx 20$, corresponds to the epoch when the first stars form. Ultraviolet radiation from these first stars and/or from the first active galactic nuclei re-ionizes the universe. Afterward, the universe is transparent in the ultraviolet.

QSOs are currently the most powerful probes of the high redshift universe. GRBs have several advantages relative to QSOs as probes of cosmology. First, GRBs are expected to occur out to $z \approx 20$, whereas QSOs occur out to only $z \approx 5$. Second, very high redshift GRB afterglows can be 100 - 1000 times brighter at early times than are high redshift QSOs. This makes possible very sensitive high dispersion spectroscopy of the metal absorption lines and the Lyman α forest in the spectrum of the afterglows. Third, no “proximity effect” on intergalactic distances scales is expected for GRBs and their afterglows, in contrast to QSOs. Thus GRBs may be rel-

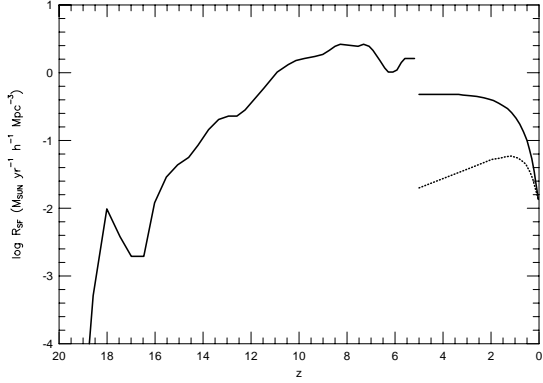


FIGURE 4. The cosmic SFR R_{SF} as a function of redshift z . The solid curve at $z < 5$ is the SFR derived by [25]; the solid curve at $z \geq 5$ is the SFR calculated by [18] (the dip in this curve at $z \approx 6$ is an artifact of their numerical simulation). The dotted curve is the SFR derived by [24]. From [15].

atively “clean” probes of the intergalactic medium, the Lyman α forest, and damped Lyman α clouds, even in the vicinity of the GRBs.

The important cosmological questions that observations of GRBs and their afterglows may be able to address include the following:

- Information about the epoch of “first light” and the earliest generations of stars from merely the detection of GRBs at very high redshifts;
- Information about the growth of metallicity in the universe in the star-forming entities in which the bursts occur, in damped Lyman α clouds, and in the Lyman α forest from observations of the metal absorption line systems in the spectra of their afterglows;
- Information about the large-scale structure of the universe at VHRs from the clustering of the Lyman α forest lines and the metal absorption-line systems in the spectra of their afterglows; and
- Information about the epoch of re-ionization from the depth of the Lyman α break in the spectra of their afterglows.

Below we consider the first of these questions: the epoch of “first light” and the earliest generations of stars.

GRBS AS A PROBE OF STAR FORMATION

Observational estimates [21,22,23,24] indicate that the SFR in the universe was about 15 times larger at a redshift $z \approx 1$ than it is today. The data at higher redshifts from the Hubble Deep Field (HDF) in the north suggests

a peak in the SFR at $z \approx 1 - 2$ [24], but the actual situation is highly uncertain.

In Figure 4, we have plotted the SFR versus redshift from a phenomenological fit [25] to the SFR derived from submillimeter, infrared, and UV data at redshifts $z < 5$, and from a numerical simulation by [18] at redshifts $z \geq 5$. The simulations done by [18] indicate that the SFR increases with increasing redshift until $z \approx 10$, at which point it levels off. The smaller peak in the SFR at $z \approx 18$ corresponds to the formation of Population III stars, brought on by cooling by molecular hydrogen. Since GRBs are detectable at these VHRs and their redshifts may be measurable from the absorption-line systems and the Ly α break in the afterglows [4], if the GRB rate is proportional to the SFR, then GRBs could provide unique information about the star-formation history of the VHR universe.

We have calculated the expected number N_* of stars as a function of z assuming (1) that the GRB rate is proportional to the SFR¹, and (2) that the SFR is that given in Figure 4 (see [15] for details). The left panel of Figure 5 shows our results for $N_*(z)$ for an assumed cosmology $\Omega_M = 0.3$ and $\Omega_\Lambda = 0.7$ (other cosmologies give similar results). The solid curve corresponds to the star-formation rate in Figure 4; the dashed curve corresponds to the star-formation rate derived by [24]. Figure 5 shows that $N_*(z)$ peaks sharply at $z \approx 2$ and then drops off fairly rapidly at higher z , with a tail that extends out to $z \approx 12$. The rapid rise in $N_*(z)$ out to $z \approx 2$ is due to the rapidly increasing volume of space. The rapid decline beyond $z \approx 2$ is due almost completely to the “edge” in the spatial distribution produced by the cosmology. In essence, the sharp peak in $N_*(z)$ at $z \approx 2$ reflects the fact that the SFR we have taken is fairly broad in z , and consequently, the behavior of $N_*(z)$ is dominated by the behavior of the co-moving volume $dV(z)/dz$; i.e., the shape of $N_*(z)$ is due almost entirely to cosmology. The right panel in Figure 5 shows the cumulative distribution $N_*(>z)$ of the number of stars expected as a function of redshift z . The solid and dashed curves have the same meaning as in the upper panel. Figure 5 shows that for the particular SFR we have assumed, $\approx 40\%$ of all stars (and therefore of all GRBs) have redshifts $z > 5$.

ESTIMATES OF THE GRB RATE

Is the GRB rate indeed proportional to the SFR (at least roughly)? We address this question in two ways. First, we

¹ This may underestimate the GRB rate at VHRs since it is generally thought that the initial mass function will be tilted toward a greater fraction of massive stars at VHRs because of less efficient cooling due to the lower metallicity of the universe at these early times.

consider the sample of GRBs with known redshifts. We adopt a Bayesian approach and calculate the likelihood of the data, assuming a very general model for the GRB rate and a power-law model for the intrinsic GRB photon luminosity distribution [26]. We fit the model jointly to the peak fluxes and redshifts of the 14 GRBs with known z , and the 7 GRBs for which there are constraints on z . Figure 6 shows our preliminary results. These suggest that the SFR models lie at about a 68% excursion from the best-fit GRB rate model. Thus we find that, despite the qualitative differences that exist between the observed GRB rate and estimates of the SFR in the universe, current data are consistent with the actual GRB rate being approximately proportional to the SFR when observational selection effects are taken into account.

Second, we use the variability of the lightcurves of long GRBs to estimate their distribution as a function of intrinsic photon luminosity and redshift [27]. Figure 7 shows the resulting joint redshift and luminosity distribution. This distribution suggests that the GRB rate continues to increase at very high redshifts, and that the intrinsic luminosities of GRBs evolve with redshift.

CONCLUSIONS

If the long GRBs are indeed produced by the collapse of massive stars, one expects GRBs to occur out to $z \approx 15 - 20$, redshifts that are far larger than those expected for the most distant QSOs. We have shown that both GRBs and their afterglows are easily detected out to these VHRs. GRBs can therefore give us information about the star-formation history of the universe, including the earliest generations of stars. The absorption-line systems and the Ly α forest visible in the spectra of GRB afterglows can be used to trace the evolution of metallicity in the universe, and to probe the large-scale structure of the universe at VHRs. Finally, measurement of the Ly α break in the spectra of GRB afterglows can be used to constrain, or possibly measure, the epoch at which reionization of the universe occurred.

REFERENCES

1. Castander, F. J., & Lamb, D. Q. 1999, ApJ, **523**, 593
2. Fruchter, A. S., et al. 1999, ApJ, **516**, 683
3. Kulkarni, S. R., et al. 1998, Nature, **395**, 663
4. Fruchter, A. S. 1999, ApJ, **516**, 683
5. Sahu, K. C., et al. 1997, Nature, **387**, 476
6. Kulkarni, S. R., et al. 1999, Nature, **398**, 389
7. Reichart, D. E., 1999, ApJ, **521**, L111
8. Galama, T. J., et al. 2000, ApJ, **536**, 185
9. Bloom, J. S., et al. 1999, Nature, **401**, 453
10. Woosley, S. E. 1993, ApJ, **405**, 273
11. Woosley, S. E. 1996, in Gamma-Ray Bursts, eds. C. A. Meegan, R. D. Preece, & T. M. Koshut (New York: AIP), 520
12. Paczyński, B. 1998, ApJ, **494**, L45
13. MacFadyen, A. I., & Woosley, S. E. 1999, ApJ, **524**, 262
14. Wheeler, J. C., et al. 2000, ApJ, **537**, 810
15. Lamb, D. Q., & Reichart, D. E., 2000, ApJ, **536**, 1
16. Wijers, R. A. M. J., Rees, M. J., & Mészáros, P. 1997, MNRAS, **288**, L51
17. Andersen, M. I., et al. 2000, A&A, **364**, L54
18. Ostriker, J. P., & Gnedin, N. Y. 1996, ApJ, **472**, L63
19. Gnedin, N. Y., & Ostriker, J. P. 1997, ApJ, **486**, 581
20. Valageas, P., & Silk, J. 1999, A&A, **347**, 1
21. Gallego, J. 1995, ApJ, **455**, L1
22. Lilly, S. J., et al. 1996, ApJ, **460**, L1
23. Connolly, A. J. 1997, ApJ, **486**, L11
24. Madau, P., Pozzetti, L., & Dickinson, M. 1998, ApJ, **498**, 106
25. Rowan-Robinson, M. 1999, Ap&SS, **266**, 291
26. Weinberg, N., Graziani, C., Lamb, D. Q., and Reichart, D. E. 2001, in Proceedings of the Rome Workshop, in press (astro-ph/010759)
27. Reichart, D. E. and Lamb, D. Q. 2001, in Proceedings of the 20th Texas Symposium on Relativistic Astrophysics, in press (astro-ph/0103255)

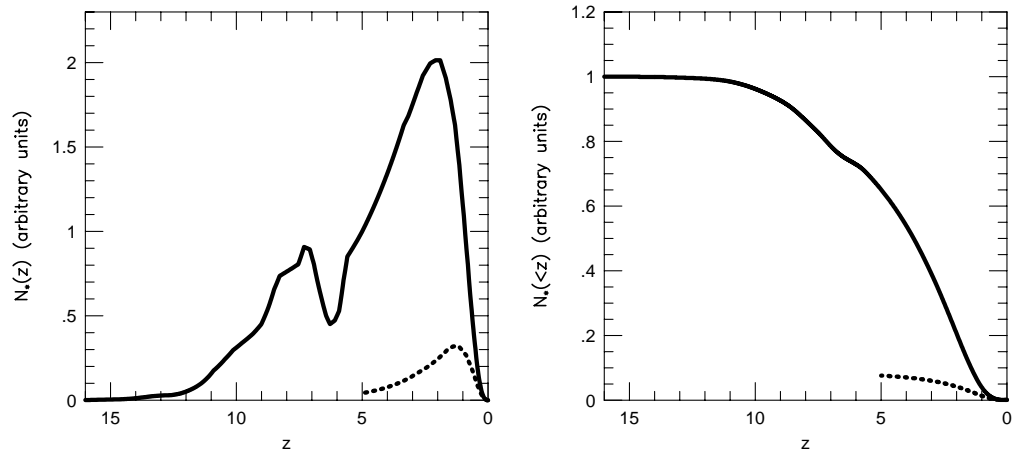


FIGURE 5. Left panel: The number N_* of stars expected as a function of redshift z (i.e., the SFR from Figure 4, weighted by the differential comoving volume, and time-dilated) assuming that $\Omega_M = 0.3$ and $\Omega_\Lambda = 0.7$. Right panel: The cumulative distribution of the number N_* of stars expected as a function of redshift z . Note that $\approx 40\%$ of all stars have redshifts $z > 5$. The solid and dashed curves in both panels have the same meanings as in Figure 4. From [15].

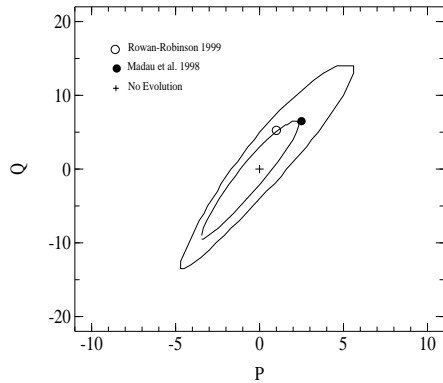


FIGURE 6. Credible regions for the GRB rate parameters P and Q . The solid curves correspond to the 68% and 95% probability contours. Also shown are the (P,Q) -values corresponding to no space density evolution, the Madau et al. [24] SFR, and the Rowan-Robinson model fit to IR, optical and UV data [25]. From [26].

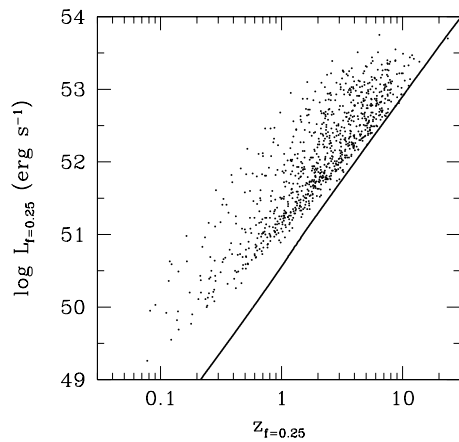


FIGURE 7. The joint redshift and luminosity distribution of the qualitatively acceptable redshift distribution (see Figure 3 in [27]). The diagonal solid line shows the 10% detection threshold of BATSE. From [27].